Proceedings of the
International Conference on Mechanical Engineering and Renewable Energy 2017
(ICMERE2017) 18 – 20 December, 2017, Chittagong, Bangladesh

ICMERE2017-PI-191

EFFECT OF IMPACT VELOCITY ON DEPOSITION BEHAVIOR FOR MICRO-SCALE GRAPHITE PARTICLES USING DRY SPRAY PROCESS

Mohammad Nur E Alam Al Nasim[1,*] and Labani Mustafi[2]

[1]School of Engineering, RMIT University, Melbourne, Victoria, Australia; email: nasim.me06@gmail.com
[2]School of Material Science and Engineering, Harbin Institute of Technology, Harbin, China; email: labani.mse@gmail.com

Abstract*-This work demonstrates the effect of impact velocity on deposition behavior of graphite microparticles during thin film preparation using dry spray deposition. Graphite microparticles were deposited using nano-particle deposition system (NPDS) by changing the impact velocities. In order to understand the co-relation between stand-off distance (the distance between the nozzle and the substrate) and impact velocity, at first computational fluid dynamics (CFD) simulations were carried out to predict the impact velocities, where impact velocities were decreased with decreased SoDs. Graphite particles were deposited by changing the impact velocities and thin films were characterized using field effect scanning electron microscopy (FE-SEM) and Raman spectroscopy analysis. The layer structured graphite particles were fragmented and interlayer separated during deposition. There is a critical velocity for interlayer separation which determines the boundary between graphite or graphene structured thin film. Apart from deposition etching/damage of deposited surfaces were observed for very high impact velocities.*

Keywords: Graphite microparticles, dry spray deposition, nanoparticle deposition system (NPDS), impact velocity, fragmentation, interlayer separation.

1. INTRODUCTION

The nanoparticle deposition system (NPDS) is a recently developed dry spray process that is used to deposit metal and ceramic particles at room temperature [1, 2]. NPDS can deposit nano- or microscale metal and ceramic particles successfully [3]. Different kinds of isotropic metal and ceramic materials such as copper, tin, nickel, NiO, Al2O3, TiO2, and WO3 have been successfully deposited by using NPDS on metal, ceramic and polymer substrates [1-3]. Recently, micro sized graphite particles were deposited on copper substrate to achieve graphene flake structured thin film [4]. Moreover, we also studied the substrate dependent deposition behaviour of graphite particles, where the deposition behavior was distinct depend on the hardness of substrates [5]. In certain flying velocity particles were fragmented into so many small pieces and interlayer separated to form graphene structures on hard substrates, where some particles didn't go under perfect fragmentation and interlayer separation to form thick graphite layer on soft substrates. So, it is needed to study the effect of different impact velocities on the deposition behaviour of graphite particles.

Previously, D.-M. Chun *et al.* [6] studied the effect of stand-off distance for cold gas spraying of micro sized ceramic particles using nanoparticle deposition system. The impact velocities of particles were calculated using computational fluid dynamics (CFD). He suggested that, the impact velocities were decreased with decreasing stand-off distance. So, the recent attempt is to study the effect of impact velocity of anisotropic layered structured graphite particles which strongly depends on the stand-off distance (SoD). At first computational fluid dynamics (CFD) simulation was carried out to predict the co-relation between stand-off distance and impact velocity. ANSYS-CFX simulation tool was used to predict the impact velocities, where impact velocities were decreased with decreased SoDs. Graphite particles of average 6 µm particles were accelerated through converging-diverging nozzle from lower to higher impact velocities by gradually increasing the SoDs for getting deposited thin films. Successfully deposited thin films were microstructurally characterized using field effect scanning electron microscopy (FE-SEM) and Raman spectroscopy. Deposition results suggest that layer structured graphite particles were fragmented and interlayer separated during deposition. There is a critical velocity for interlayer separation which defines the boundary between layered graphite or graphene structured thin film. The critical velocity for graphene structured thin film preparation lies between 250 ms^{-1} and 260 ms^{-1}. The original graphite particles didn't undergo perfect fragmentation and interlayer separation below this critical velocity. In contrast, above this critical velocity, fragmentation and interlayer separation of deposited particles were gradually increased with increased impact velocities. Besides successful deposition etching/damage of substrates were observed

with very high impact velocities. So, in this research the co-relation between impact velocities and surface morphologies of deposited thin films were carefully studied to get graphite/graphene flake structured thin film for future applications

2. EXPERIMENTAL

Experimentally it is not possible to get the impact velocity of particles using cold gas spray or dry spray deposition because of bow shock or an increasing pressure gradient near the substrate. Pattison *et al*. [7] used particle image velocimetry (PIV) to know the flying velocity of particles. They found that particles average flying velocity and impact velocity didn't differ so much in cold gas spray as the particle momentum is high enough for the particle velocity near the substrate to change. However, small particles are affected by the bow shock or an increasing pressure gradient near the substrate. So, in this research at first we followed a computational fluid dynamics (CFD) analysis to predict the impact velocity of graphite particles. CFD analysis was carried out using a commercially available CFD tool, ANSYS CFX (V 15). CFX supports Lagrangian tracking for simulation of particle movement in a flow. The boundary conditions were strictly maintained as followed by D.-M. Chun et al. [6] except the properties of graphite particles. To confirm the reduction of velocity near to the substrate for graphite particle, CFD analysis was carried out by taking 5-7 µm graphite particles. The proper material properties of graphite (density, specific heat capacity) were chosen for CFD analysis [8]. Fig. 1(a) shows the CFD model and 1(b) shows the velocity profile of the particles and flow for 5-7 µm graphite particles, where the stand-off distance is 1 mm. The obtained flow velocity was normal to the substrate along the nozzle. The impact velocity of 5-7 µm graphite particles was decreased near to the substrate and the velocity profile trend of the particles was same as flow velocity and the velocity decreased near to the substrate, as shown in Fig. 1(b).

Fig. 2 (a) shows the velocity results of fluid around the nozzle. The maximum flow velocity was 602 ms^{-1} and along the nozzle the flow velocity continuously increased. But outside the nozzle the flow velocity was suddenly decreased due to the substrate. Pressure gradient was also involved for decreased flow velocity near to the substrate. Fig. 2(b) shows the pressure distribution around the nozzle. The pressure along the nozzle was decreased gradually from 396 kPa. Interestingly, near to the substrate the pressure was increased due to bow shock as shown in Fig. 2(b). This bow shock was responsible for decreased particle velocity near to the substrate.

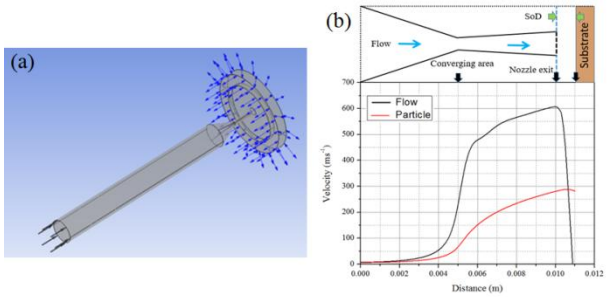

Fig. 1 (a) CFD model and (b) Velocity profile of the particles and flow along the nozzle center line for 5-7 µm graphite particles.

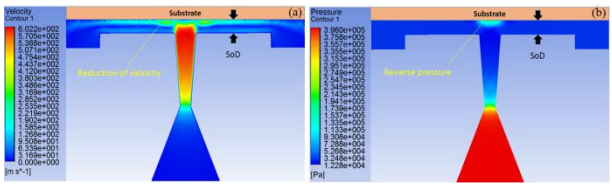

Fig. 2 CFD visualization- (a) flow velocity and (b) pressure distribution results around the nozzle.

As impact velocity depends on the SoD and shape of the nozzle, at first four different kinds of SoDs such as 0.5 mm, 1 mm, 3 mm, 5 mm, 7 mm and 10 mm were considered for 5-7 µm graphite particles. The circular nozzle was used to study the effect of SoD on the impact velocity. The boundary conditions of CFX model were provided in Table 1 and the calculated impact velocities for different SoDs were given in Table 2. It was observed that with increasing the SoDs the impact velocities were increasing, where there was no significant difference between 5 mm and 7 mm SoDs. So, Experimentally in order to study the deposition behavior of graphite particles for different impact velocities, five different SoDs uuch as- 0.5 mm, 1 mm, 3 mm, 5 mm and 10 mm were considered for deposition. The experimental data were provided in Table 3. Deposited thin films were characterized using field effect scanning electron microscopy (FE-SEM) and Raman spectroscopy analysis.

Table 1: CFD boundary conditions.

Feedstock material	Graphite powder, 5-7 µm
Particle properties	Density (2260 kgm^{-3}), Specific heat capacity (0.71 $Jg^{-1}k^{-1}$)
Nozzle dimension	Circular Nozzle, Length 50 mm, Converging diameter 0.8 mm
Carrier gas pressure	3 Bar
Chamber pressure	210 Torr
Spray angle	90^{o} (Normal to substrate)
Distance between substrate and nozzle	0.5 mm, 1 mm, 3 mm, 5 mm, 7 mm and 10 mm

Table 2: Calculated impact velocities of circular nozzle for variable SoDs.

SoD (mm)	**0.5**	**1**	**3**	**5**	**7**	**10**
Average impact velocity (ms^{-1})	250	260	290	299	300	442

Table 3: Process parameters for graphite deposition

Feedstock material	Graphite powder, 5-7 µm, (MGF 6 995A, Samjung CNG, Korea)
Substrate	Cu foil (CU-113303, Nilaco Corporation, Japan)
Nozzle	Circular Nozzle, 0.8 mm (converging diameter)
Distance between substrate and nozzle	0.5 mm, 1 mm, 3 mm, 5 mm and 10 mm
Career gas pressure	3 Bar
Vacuum level	210 Torr
Gas flow rate	9.5 l/min
Scanning speed	0.02 mm/s

3. RESULTS AND DISCUSSION

3.1 Surface morphologies

The surface morphologies of original graphite particles and deposited thin films were characterized using FE-SEM. The original graphite particle was shown in Fig. 3. The particle size was about 6 µm and the shape of the graphite was not regular.

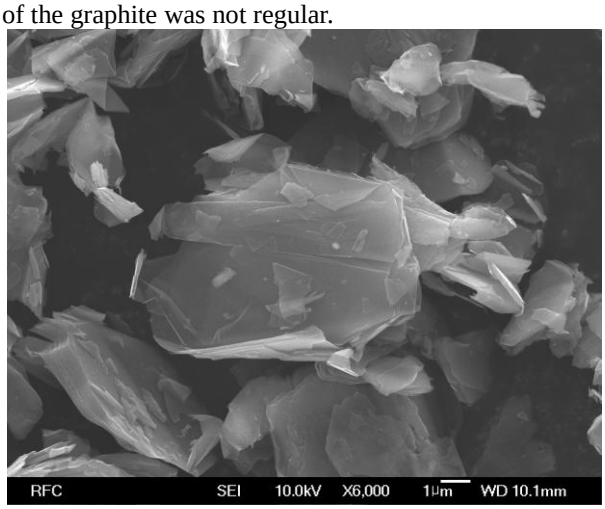

Fig. 3 FE-SEM image of original graphite particles.

The deposited thin films were evaluated with FE-SEM. The FE-SEM images of deposited thin film on Cu substrate were shown in Fig. 4. It is clear that the particle sizes in deposited thin films are smaller than the size of original graphite powder by comparing Fig. 3 and Fig. 4 irrespective of impact velocities. For lowest impact velocity i.e. 250 ms^{-1}, some particles were cracked into so many small pieces during deposition and some particles were experienced less fragmentation partially as shown in Fig. 4(a). Less fragmented and deformed flakes were clearly visible in the right panel of Fig. 4(a) with high magnified view. Interestingly, when the impact velocity was higher such as- 260 ms^{-1}, al the particles were fragmented into small pieces as shown in Fig. 4(b). For 260 ms^{-1} velocity, no less fragmented particles were observed even in the high magnified image of the right panel of Fig. 4(b). Similarly at 290 ms^{-1} impact velocity, severe fragmentation was observed as shown in Fig. 4(c). It's difficult to know the exact grain size information from high magnified image as shown in right panel of Fig. 4(c). In contrast, distinct surface morphologies were observed at very high impact velocities as shown in Fig. 4(d) and 4(e). For example, at 299 ms^{-1} and 422 ms^{-1} impact velocity, apart from severe fragmentation etching/damage of copper substrate was happened. Those damages happened due to high impact velocities of graphite particles. In the etched/damaged portion, the fragmented flakes were visible too, which were shown in right side panel of Fig. 4(d) and 4(e). Interestingly, by comparing Fig. 4(d) and 4(e) it is clear that, the amount of etching/damage was higher for 442 ms^{-1} than 299 ms^{-1}. From above discussion, it can be said that only the surface morphology can't define the graphite or graphene state of deposited thin films.

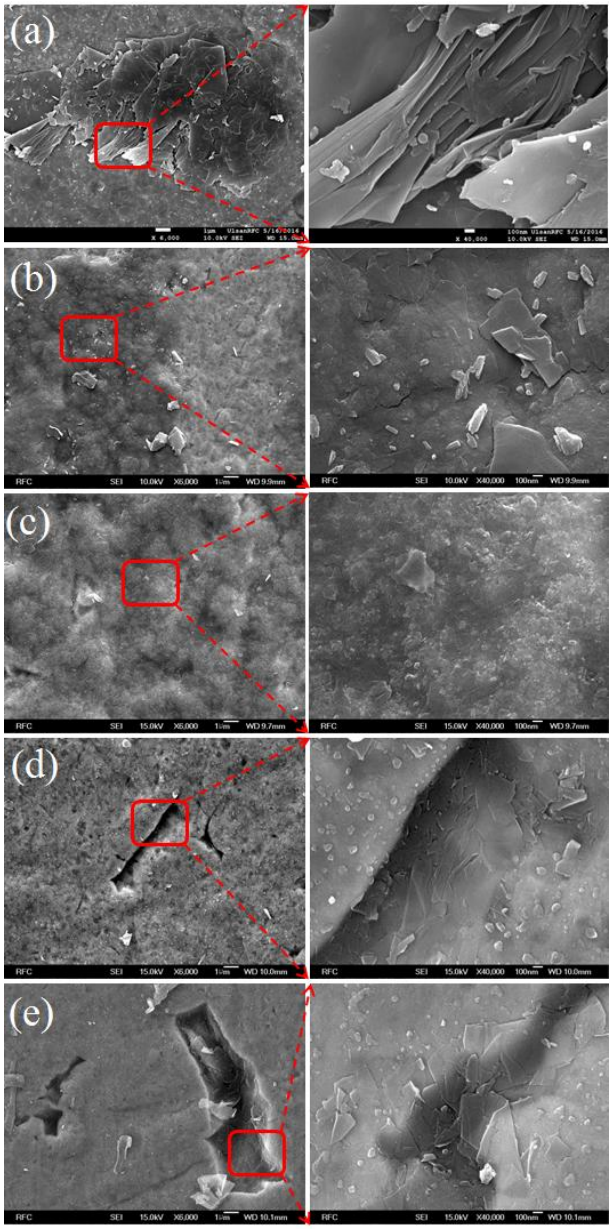

Fig. 4 FE-SEM images of deposited thin films on Cu substrate for (a) 250 ms^{-1}, (b) 260 ms^{-1}, (c) 290 ms^{-1}, (d) 299 ms^{-1} and (e) 442 ms^{-1}.

3.2 Raman spectroscopy analysis

To confirm the graphite and graphene structures of the deposited thin films, a confocal micro-Raman apparatus (Alpha 300R, WITec, Germany) was used to carry out Raman spectroscopic analysis. The original graphite powder and the thin films deposited on copper substrate were analyzed in Fig. 5. The band range evaluated was between 1000 and 3000 cm^{-1}, which includes the main features in Raman spectra of carbon-based materials such as- D, G, and 2D peaks. In the Raman spectrum for the original graphite powder, the most intense band was the G peak, located at ~1582 cm^{-1}, and a band at ~2721 cm^{-1}, historically referred to as the 2D band [9-13]. The 2D peak of graphite particles consists of two components, $2D_1$ and $2D_2$, as shown in Fig. 5. Some researchers already explained the double structure of the 2D peak in graphite [11, 14-18]. The disorder peak named as D of graphite was located at ~1352 cm^{-1}, which represents highly ordered crystalline structure due to its negligible intensity of D peak. However the Raman spectra of the thin films deposited on Cu substrates varied considerably, as the depositions were carried out with varying impact velocities. Table 4 summarizes the G and 2D peak positions of the graphite powder and of the deposited thin films for various impact velocities.

Less fragmented graphite particles deposited on copper substrate at 250 ms^{-1}. When the laser was focused on less fragmented and deformed particles, the D, G, and 2D band peaks were at ~1352, ~1582 and ~2720 cm^{-1} respectively, similar to the peak positions of the original graphite powder. The graphitic-shaped 2D bands and increased D (disorder) band intensities of this film relative to the original graphite (Fig. 5) suggested that during deposition, large graphite particles were cracked into small pieces to make a relatively thick film of randomly oriented flakes in which the graphitic crystal structures were maintained. The thin film on the copper substrate showed two distinct behaviors for 250 ms^{-1} as discussed in the corresponding FE-SEM results at section 3.1. When the laser beam was focused on the area containing fragmented, fine particles (recall Fig. 4a), the resulting Raman spectrum included an intense disorder band (Fig. 5). The peak intensity of the disorder band D was stronger than that of G peak (i.e., I_D/I_G was much higher than that of the graphite powder). This means that intense fragmentation occurred after deposition due to the high impact velocity, and that the deposited particles were featured with defected flakes. The G and 2D bands are the most important features of the Raman spectrum for graphene structure in deposited thin films. The G and 2D peaks were at ~1586 and ~2694 cm^{-1}, respectively. The fragmented fine particles clearly yielded a higher-energy G peak and a lower-energy 2D peak compared to those of the original graphite powder (Fig. 5). The significant shifts observed in the G and 2D peaks (indicated by arrows in Fig. 5), as well as the differences in the shapes and intensities of the 2D peaks, indicate the different materials of graphene and bulk graphite [11, 13]. The 2D band of the deposited thin film became sharper than the original graphite powder in the fragmented area with separated interlayers. Moreover, the upward shift in the G peak and the downward shift in the 2D peak in that area indicated that the deposited graphene flakes were thinner than the original graphite powder after deposition (Fig. 5). The G peak was accompanied by a shoulder peak at ~1620 cm^{-1} (D′ band), as shown in Fig. 5. This D′ band suggests symmetry breaking defect associated graphene flakes and the origin of this peak may be due to the intravalley double resonance Raman process [19].

For 260 ms^{-1}, 290 ms^{-1}, 299 $ms^{-1}$and 422 ms^{-1} the deposited thin films on copper substrates, the D peaks were also highly intense; also, the G position was shifted up and the 2D position was shifted down, as shown in Fig. 5. For higher velocities more fragmentation and interlayer separation was happened, as the G and 2D peaks were shifted accordingly. The shoulder peak (D′) position was similar for the deposited films of all impact velocities. For severe damage of substrates at impact

velocities of 299 ms^{-1} and 422 ms^{-1}, the deformed and fragmented flakes also appeared as graphene flake structures, because the Raman peak positions satisfied the graphene specification. In conclusion, based on the shifts in the G and 2D peaks, layers of microscale graphite powder particles were separated due to the high-velocity impact during deposition, and very thin few-layer graphene structures were formed on copper substrates at 260 ms^{-1}, 290 ms^{-1}, 299 ms^{-1} and 442 ms^{-1}, whereas at 250 ms^{-1} impact velocity it revealed both graphite and graphene structures [11, 13]. Moreover, the strong and sharp D band peak and D′ band peak suggested nanocrystalline structures as well as the presence of graphene edges and defects. These nanocrystalline structures, graphene edges and defects may have increased with increasing substrate hardness. And these defects might have occurred during high-impact-velocity deposition by means of interactions between the substrates and graphene, which may produce vacancies, dislocations, and/or dangling bonds [12, 20-22].

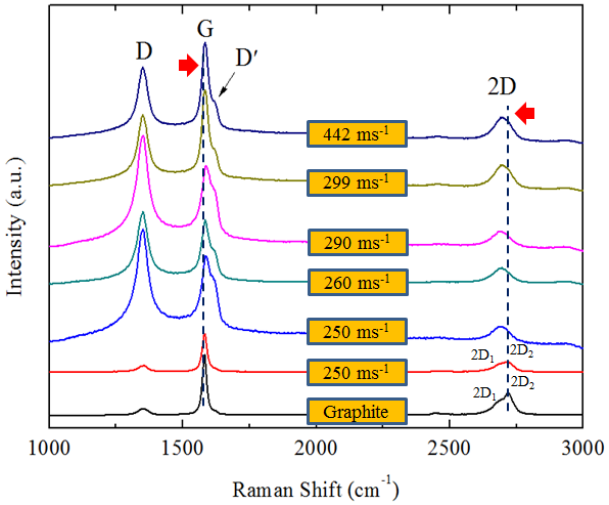

Fig. 5 Raman spectrum of deposited thin films at different impact velocities such as- 250 ms^{-1}, 260 ms^{-1}, 290 ms^{-1}, 299 ms^{-1} and 442 ms^{-1}.

Table 2: G and 2D peak positions of graphite powder and deposited thin films at different impact velocities.

Material/thin film according to impact velocities	**G Peak position (cm^{-1})**	**2D Peak position(cm^{-1})**
Graphite powder	1582	2720
250 ms^{-1} (graphitic structure)	1582	2720
250 ms^{-1} (graphene structure)	1586	2694
260 ms^{-1}	1586	2694
290 ms^{-1}	1588	2692
299 ms^{-1}	1585	2694
442 ms^{-1}	1586	2694

4. CONCLUSION

Room-temperature dry spray depositions of microscale graphite particles were deposited on copper substrates at different impact velocities. Impact velocities were changed by changing the stand-off distance during deposition. To predict the impact velocities CFD simulations were carried out. CFD results predicted that with increasing stand-off distances, the impact velocities were increased. According to impact velocities, deposited thin films were characterized and it was found that the suitable impact velocity for graphene structured thin film lies between 250 ms^{-1} and 260 ms^{-1}. Very high impact velocity caused severe etching/damage of substrates. So, this research gave us a conclusion about the choosing of impact velocity for graphite/graphene structured thin film fabrication.

5. ACKOWLEDGEMENT

This research was supported by the special research grant of the school of mechanical engineering at University of Ulsan, South Korea.

6. REFERENCES

1. Chun, D.-M. and S.-H. Ahn, Deposition mechanism of dry sprayed ceramic particles at room temperature using a nano-particle deposition system. Acta Materialia, 2011. 59(7): p. 2693-2703.
2. Chun, D.-M., et al., Nano-particle deposition system (NPDS): low energy solvent-free dry spray process for direct patterning of metals and ceramics at room temperature. International Journal of Precision Engineering and Manufacturing, 2012. 13(7): p. 1107-1112.
3. Kim, H., et al., Effect of particle size on various substrates for deposition of NiO film via nanoparticle deposition system. Thin Solid Films, 2016. 600: p. 109-118.
4. Al Nasim, M.N.E.A. and D.-M. Chun, Formation of few-layer graphene flake structures from graphite particles during thin film coating using dry spray deposition method. Thin Solid Films, 2017. 622: p. 34-40.
5. Al Nasim, M.N.E.A. and D.-M. Chun, Substrate-dependent deposition behavior of graphite particles dry-sprayed at room temperature using a nano-particle deposition system. Surface and Coatings Technology, 2017. 309: p. 172-178.
6. Chun, D.-M., et al., Effect of stand-off distance for cold gas spraying of fine ceramic particles (< 5μm) under low vacuum and room temperature using nano-particle deposition system (NPDS). Surface and Coatings Technology, 2012. 206(8): p. 2125-2132.
7. Pattison, J., et al., Standoff distance and bow shock phenomena in the Cold Spray process. Surface and Coatings Technology, 2008. 202(8): p. 1443-1454.

8. Pierson, H.O., Handbook of carbon, graphite, diamonds and fullerenes: processing, properties and applications. 2012: William Andrew.
9. Jeon, C.-S., et al., Mechanical properties of graphite/aluminum metal matrix composite joints by friction stir spot welding. Journal of Mechanical Science and Technology, 2014. 28(2): p. 499.
10. Wang, Y., D.C. Alsmeyer, and R.L. McCreery, Raman spectroscopy of carbon materials: structural basis of observed spectra. Chemistry of Materials, 1990. 2(5): p. 557-563.
11. Ferrari, A.C., Raman spectroscopy of graphene and graphite: disorder, electron–phonon coupling, doping and nonadiabatic effects. Solid state communications, 2007. 143(1): p. 47-57.
12. Ni, Z., et al., Raman spectroscopy and imaging of graphene. Nano Research, 2008. 1(4): p. 273-291.
13. Wang, H., et al., Vibrational properties of graphene and graphene layers. Journal of Raman Spectroscopy, 2009. 40(12): p. 1791-1796.
14. Cançado, L., et al., Anisotropy of the Raman spectra of nanographite ribbons. Physical review letters, 2004. 93(4): p. 047403.
15. Nemanich, R. and S. Solin, First-and second-order Raman scattering from finite-size crystals of graphite. Physical Review B, 1979. 20(2): p. 392.
16. Vidano, R., et al., Observation of Raman band shifting with excitation wavelength for carbons and graphites. Solid State Communications, 1981. 39(2): p. 341-344.
17. Pócsik, I., et al., Origin of the D peak in the Raman spectrum of microcrystalline graphite. Journal of Non-Crystalline Solids, 1998. 227: p. 1083-1086.
18. Maultzsch, J., et al., Phonon dispersion in graphite. Physical review letters, 2004. 92(7): p. 075501.
19. Beams, R., L.G. Cançado, and L. Novotny, Raman characterization of defects and dopants in graphene. Journal of Physics: Condensed Matter, 2015. 27(8): p. 083002.
20. Hiramatsu, M., et al., Fabrication of vertically aligned carbon nanowalls using capacitively coupled plasma-enhanced chemical vapor deposition assisted by hydrogen radical injection. Applied physics letters, 2004. 84(23): p. 4708-4710.
21. Hiramatsu, M. and M. Hori, Fabrication of carbon nanowalls using novel plasma processing. Japanese journal of applied physics, 2006. 45(6S): p. 5522.
22. Mori, T., et al., Fabrication of carbon nanowalls using electron beam excited plasma-enhanced chemical vapor deposition. Diamond and Related Materials, 2008. 17(7): p. 1513-1517.